results in
PHYSICS

Heat treatment and kinetics of precipitation of β-Mg$_{17}$Al$_{12}$ phase in AZ91 alloy

M. Fatmi[a], A. Djemli[a,b], A. Ouali[b], T. Chihi[a,*], M.A. Ghebouli[a], H. Belhouchet[c]

[a] Research Unit on Emerging Materials (RUEM), Ferhat Abbas of Setif 01, Setif 19000, Algeria
[b] Department of Physics, Faculty of Science, University Mohamed Boudiaf of M'sila, 28000 M'sila, Algeria
[c] Physics and Chemistry of Materials Lab, Department of Physics, University Mohamed Boudiaf of M'sila, 28000 M'sila, Algeria

ABSTRACT

This study investigated the effect of aging on the precipitation and kinetics of second phase Mg$_{17}$Al$_{12}$ in AZ91 magnesium alloy (Mg-9 wt% Al-1 wt% Zn), using X-ray diffraction, microhardness measurements and differential scanning calorimetric analysis (DSC). With the last instrument, the all samples were heated from room temperature to 400 °C, at heating rates of 10–30 °C/min. The results were supplemented by measuring the average of activation energies, using isothermal treatments by Johnson–Mehl–Avrami (JMA) methods and by non-isothermal treatments using Ozawa, Boswell, Kissinger, Mahadevan, Augis and Bennett methods, were around 67.18 and 62.02 kJ/mol. The frequency factor k_0 calculated by the isothermal treatment is equal to 1.24 $10^9 s^{-1}$. In non-isothermal treatment, the numerical factor m and the Avrami parameter n is estimated to be approximately equal to 3 and 2.79 respectively. This value corresponding that the bulk nucleation with a constant number of nuclei was dominant in three-dimensional (polyhedron) controlled by interface reaction.

Introduction

The magnesium is the lightest element among metals used as a structural alloy. These alloys are characterized by a low density, a strong corrosion resistance; they improve the capacity of damping ability and show adequate mechanical properties. In this type of alloy, the aluminum is the main element because of its low cost and presents advantageous effects on the properties of strength and corrosion. The aforementioned properties are the main reasons which lead to the use of these alloys in the automobile, the aerospace industry, the industry of electronics and the industries of weapons as guides arm [1–3]. Various alloys with Mg are developed for applications by alloying with major elements such as Al, Mn, Zn, Zr, Y, etc… The alloy called AZ91, which contains about 9 wt% Al, 1 wt% Zn, with the addition of 0.4 wt% Mn is the most widely used magnesium alloy. It exhibits a good combination of high strength at room temperature, good cast ability and excellent corrosion resistance [4–6].

The alloy AZ91 can exist in two different phases, the first one is the α-phase which is a solid solution, whereas the second is β-(Mg$_{17}$Al$_{12}$). This latter phase consists of Mg and Al. The addition of Zn to the Mg-Al alloy system contributes to the reduction of the solid solubility of Al in Mg [7,8]. The addition large quantities of Al cause the ductility to decrease through the formation of a breakable intermetallic phase

(typically, Mg$_{17}$Al$_{12}$), zinc usually takes the place of Al in Mg$_{17}$Al$_{12}$ in AZ91, forming a ternary intermetallic compound Mg$_{17}$(Al,Zn)$_{12}$ [3,6]. Silicon tends to produce hard Mg$_2$Si precipitating at grain boundaries, enhancing creep strength at high temperatures [9]. According to the phase diagram of the Mg-Al binary alloy, the maximum solid solubility of aluminum in magnesium is practically high at 12.9 wt% Al (at the eutectic temperature of 437 °C). The equilibrium phase precipitates have a stoichiometric composition of Mg$_{17}$Al$_{12}$ (44.0 wt% Al) and an α-Mn-type cubic unit cell (space group $1\bar{4}3m$). The lattice parameter for the stoichiometric Mg$_{17}$Al$_{12}$ phase is 1.056 nm [10]. The β phase precipitation is different from the precipitation in Al alloys. The content of Al also influences the amount of Mg$_{17}$Al$_{12}$ intermetallic phase particles, which affects the corrosion processes. The influence of Mg$_{17}$Al$_{12}$ particles on the alloy corrosion properties depends on their amount, morphology, and distribution in the alloy structure [11].

Azzeddine et al. [12] in a study of the kinetics of precipitation in AZ91 alloy by in situ X-ray diffraction; they found that the macroscopic kinetics of the discontinuous precipitation at 200 °C was determined via the integral intensity and also by Vickers microhardness measurements. They found that the macroscopic kinetics can be well described by the Johnson-Mehl-Avrami law and that the n Avrami parameter indicates that the precipitation proceeds by a mechanism of nucleation after site saturation. In the AZ91 alloy, the phenomenon of structural hardening

---

is due to the precipitation reaction but this hardening is not important compared to the Al-Zn alloys, because of the appearance of types of reactions continuous and discontinuous precipitations. The first hardens the material while the second is responsible for its softening. The discontinuous precipitation produces, locally from the grain boundary, a duplex cellular structure formed of alternating lamellae of the $Mg_{17}Al_{12}$ phase (Tu and Turnbull Model) [13], and solute-depleted solid solution while the continuous precipitation corresponds to germination and growth of particles of the solute. Same phase $Mg_{17}Al_{12}$ precipitated but in the form of rods or platelets in a massive into the grain interior [14,15]. In this alloy, continuous precipitation is favored at high and low temperatures, while discontinuous precipitation dominates at intermediate temperatures [15]. On the other hand, after heating a supersaturated solid solution from room temperature to 665 K both discontinuous and continuous precipitates were observed simultaneously [16,17]. Our present work contains various calculated kinetic parameters of precipitation of new β-($Mg_{17}Al_{12}$) phase. The measured parameters have been used the five methods of Ozawa, Bozwal, mahadavan, Augis and Bennett and Kissenger under non-isothermal condition using the Differential Scanning Calorimetry analysis (DSC).

Experimental procedure

The composition of the AZ91 alloy prepared for this work is given in Table 1. All specimens used for the experiments were covered by graphite powder to limit oxidation, which happens quickly above 370 °C [5,18]. The solution-treated at 420 °C for 4 h and subsequently water quenched. The tested samples were machined from the homogenized alloy. They have been cut in a disc form of 7 mm of diameter and 4 mm of height, having an average weight of 300 mg. Differential scanning calorimetry (DSC) analysis of the samples was performed in a purified argon atmosphere, using an SDT Q 600 DSC Analyzer instrument. High purity of Magnesium, aluminum and Zinc (99.999) are used as a reference material. Temperature scans were made from 20 to 420 °C with constant heating rates of 10–30 °C/min. The X-ray diffraction analysis was performed by a "PAN Analytical X' Pert PRO" diffractometer using Cu-K_α radiation, scanned at a speed of 0.9 °C/min. For mechanical characterization using the PHILIPS PW 1710 powder instrument.

Results and discussion

Non-isothermal method

The kinetics of crystallization in the metallic phases has been intensively studied can be empirically described by the classical Johnson-Mehl-Avrami (JMA) equation [19]:

$$x = 1 - \exp[(-kt)^n] \tag{1}$$

where x: is the volume fraction crystallized after time t.
n: the dimensionless quantity named the Avrami exponent.

k: the rate constant which is given by Arrhenius equation:

Table 1
Major alloying elements and their composition in the studied alloy.

Element	Composition (wt.%)
Mg	89.02
Al	9.45
Zn	1.03
Mn	0.4

$$k = k_0 \exp\left(-\frac{E_A}{RT}\right) \tag{2}$$

where: k_0: frequency factor.
E_A: the activation energy.
R: gas constant.
T: Kelvin temperature.

The temperature is changed linearly with time at a known scan rate $v = dT/dt$, where $T = T_0 + vt$, (T_0 the starting temperature).
The Johnson-Mehl-Avrami (JMA) equation becomes:

$$x = 1 - \exp\left[-\left(\frac{k(T-T_0)}{v}\right)^n\right] \tag{3}$$

and Eq. (2) becomes:

$$k = k_0 \exp\left(-\frac{E_A}{R(T_0 + vt)}\right) \tag{4}$$

Bansal et al. [20] improved In the maximum of the peak of Eq. (1) $T = T_P$

$$\frac{d^2x}{dt^2} = 0 \tag{5}$$

Eqs. (4) and (5) into Eq. (3) gives:

$$\text{In}\left(\frac{v}{(T_P - T_0)}\right) = -\frac{E_A}{RT_p} + \text{In}(R_0) \tag{6}$$

Under the condition $T_P >> T_0$ gives:

$$\ln\left(\frac{T_p^2}{v}\right) = \ln\left(\frac{E_A}{R}\right) - \ln k + \frac{E_A}{RT_P} \tag{7}$$

In this work, the calculations of activation energy E_A of the formation of β ($Mg_{17}Al_{12}$) phase precipitate according to Eqs. (6) and (7), by Augis and Bennett Eq. (8) [18] and Kissinger methods Eq. (9) [21,22], Boswell Eq. (10) [23], Mahadevan Eq. (11) [24] and Ozawa Eq. (12) [25]; were listed respectively by the formulas:

$$y = \ln\left(\frac{v}{T_p - T_c}\right) = -\frac{E_A}{RT_p} + C_4 \tag{8}$$

$$y = \ln\left(\frac{v}{T_p^2}\right) = -\frac{E_A}{RT_p} + C_5 \tag{9}$$

$$y = \ln\left(\frac{v}{T_p}\right) = -\frac{E_A}{RT_p} + C_2 \tag{10}$$

$$y = \ln(v) = -\frac{E_A}{RT_p} + C_3 \tag{11}$$

$$y = \ln(v) = -1,0518\frac{E_A}{RT_p} + C_1 \tag{12}$$

where C_1, C_2, C_3, C_4 and C_5 are constants, v is the heating rate, E_A is the activation energy, T_P is the temperature at DSC-curve maximum and T_C the onset of temperature of crystallization.

Fig. 1, shows the typical isothermal DSC experiment curves heating from room temperature to 400 °C at a heating rate of 10–30 °C/min. The DSC scan shows an exothermic peak which corresponds to the formation of $\beta - (g_{17}Al_{12})$ phase [9,10]. The temperature is changed linearly with time at a known scan rate $v = dT/dt$.

In fact, we noticed that the peak moves towards higher temperatures as the heating rate increases. This can be attributed to two possible effects. The first comes from the decrease of the precipitated aluminum (Al) atoms amount due to the higher solid solubility at higher temperatures and higher heating rates, while the second is
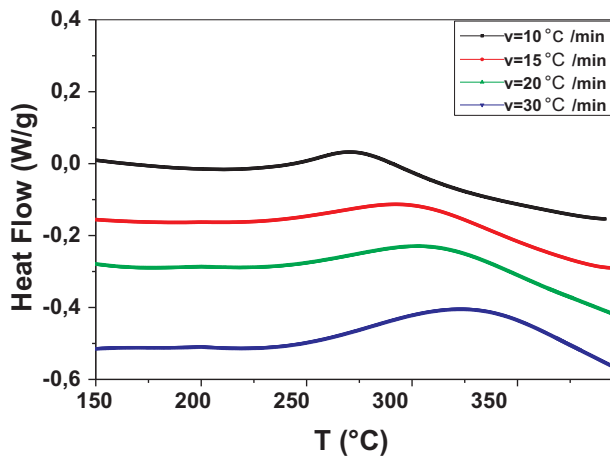
Fig. 1. DSC curves of AZ91 alloy quenched and aged at different heating rates 10, 15, 20 and 30 °C/min.
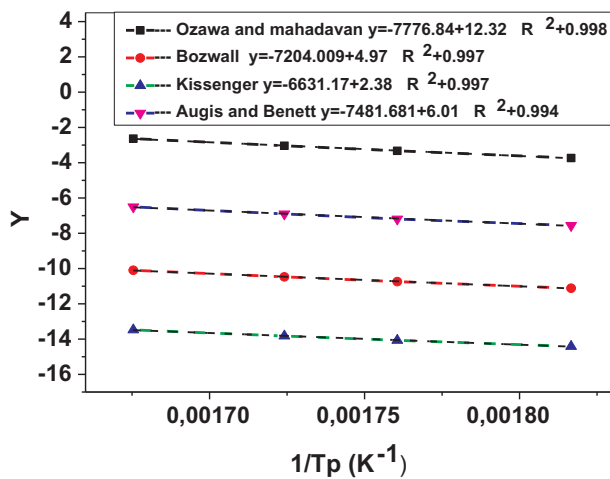

Fig. 2. $Y = f(1 = Tp)$ curves of AZ91 alloy using four different methods for the β-($Mg_{17}Al_{12}$) phase.

Table 2
The values of activation energies of β-($Mg_{17}Al_{12}$) phase formation in AZ91 alloy.

Method	E_A/(kJ/mol)	R^2
Ozawa	67.851	**0.998**
Bozwal	59.89	**0.997**
Mahadavan	64.62	**0.998**
Augis and Bennett	62.62	**0.994**
Kissenger	55.131	**0.997**

Table 3
Values of Avrami parameter n for different heating rates.

v (°C·min^{-1})	Tp (°C)	ΔTp	n
10	277.47	39.42989	2.89868224
15	295	42.62834	2.85467791
20	307	45.4553	2.79145302
30	323.87	50.6972	2.65054018

associated with the diffusive nature of the precipitation reactions [25,26]. The values of activation energies E_A can be obtained from the slop of y versus $1/T_p$ plots (Fig. 2) resulting from the curves slopes lines and the coefficient of determination R^2 are listed in Table 2. The Avrami equation describes how solids transform from one phase (state of
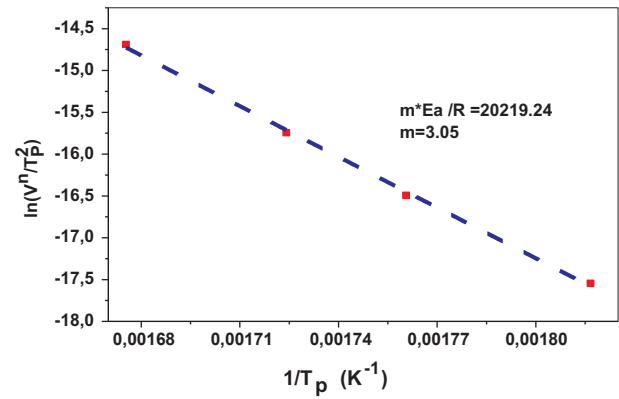
matter) to another at a constant temperature. It can specifically describe the kinetics of crystallization, can be applied generally to other changes of phase in materials, like chemical reaction rates, and can even be meaningful in analyses of ecological systems. By different methods reported previously can estimate the value of the Avrami exponent n for different heating rates (Table 3) by relation Eq. (13):

$$n = \frac{2,5T_p^2 R}{\Delta T_p E_A} \tag{13}$$

where ΔT_p is the width at half height in peaks of the DSC curves of AZ91 alloy quenched and aged at different heating rates 10, 15, 20 and 30 °C/min.

The Eq. (14) proposed by Kissinger was modified by Matusita et al. [27]:

$$\ln\left(\frac{v^n}{T_P^2}\right) = C_3 - \frac{mE_A}{RT_p} \tag{14}$$

where n the Avrami parameter indicates the precipitate mode of crystallization and m is a numerical factor, depends on the growth and dimensions of the crystallized phases. Fig. 3 shows the slope of the curve ln (v^n/ T_p) versus $1/T_p$ which is the numerical factor m. The value obtained by numerical factor m is found equal to 3.05. The growth morphology parameters n and m were both found to be equal to 3 demonstrating that bulk nucleation with a constant number of nuclei was dominant in three-dimensional (polyhedron) controlled by interface reaction. Fig. 4, show the volume fraction crystallized versus time (t) for different heating rates determined from the DSC curves by the formula below:

Fig. 3. Plot of $\ln(v^nT_p)$ versus 1/Tp according to Matusita Method.
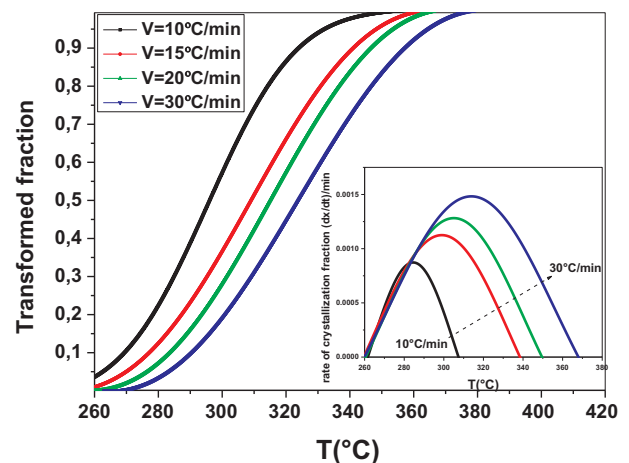

Fig. 4. Transformed fraction as a function of the temperature of AZ91 alloy quenched and aged at different heating rates 10, 15, 20 and 30 °C/min.

$$x = \frac{A_T}{A_0} \tag{15}$$

A_0 is the total area of the peak in the DSC curve between the temperature T_c (the initial of crystallization) and T_f (the completion of crystallization). A_T is the area under the peak between T_c and T. The transformations are often seen to follow a characteristic S-shaped, or sigmoidal, profile where the transformation rates are low at the beginning and the end of the transformation but rapid in between [28]. The initial slow rate can be attributed to the time required for a significant number of nuclei of the new phase to form and begin growing. During the intermediate period, the transformation is rapid as the nuclei grow into particles and consume the old phase while nuclei continue to form in the remaining parent phase.

Once the transformation approaches completion there remains little untransformed material for further nucleation and the production of new particles begins to slow. Additionally, the previously formed particles begin to touch one another, forming a boundary where growth stops.

Isothermal method

The isothermal aging is of obvious interest, which is the possibility of following the precipitation phenomenon that causes aging. From the Differentiation of Eq. (1) of Johnson-Mehl-Avrami (JMA) [19] and taking double logarithm of Eq. (1) gives:

$$\left(\frac{dx}{dt}\right) = nk^n t^n (1-x) \tag{16}$$

$$\ln[-\ln(1-x)] = n\ln(k) + n\ln(t) \tag{17}$$

$$\ln\left(\frac{dx}{dt}\right) = \ln[K_0 n] + \frac{n-1}{n}\ln[-\ln(1-x)] + \ln(1-x) - \frac{E_A}{RT}$$
$$= \ln[k_0 f(x)] - \frac{E_A}{R.T} \tag{18}$$

The plot of $\ln(dx/dt)$ and $1/T$ against x is shown in Fig. 5, by every different heating rates the slope of plot $\ln(dx/dt)$ versus $1/T$ at same value of crystallized fraction x we can obtain the activation energy of isothermal method by Ligero et al. (Table 4), and select many pairs of x_1 and x_2 for found the value of avrami exponent n. From a mathematical method through non-isothermal technique, Ligero et al. have found that the slope of the linear relation of Eq. (18) shown in (Fig. 6). If we selected the same value of x (transformed fraction) in every different heating rate, we can be deduced the activation energy E_A. all values is listed in Table 4.

For determinate the Avrami exponent n by select two pair points of x_1 and x_2 by providing $\ln[k_0 f(x_1)] = \ln[k_0 f(x_2)]$ into Eq. (18) gives:
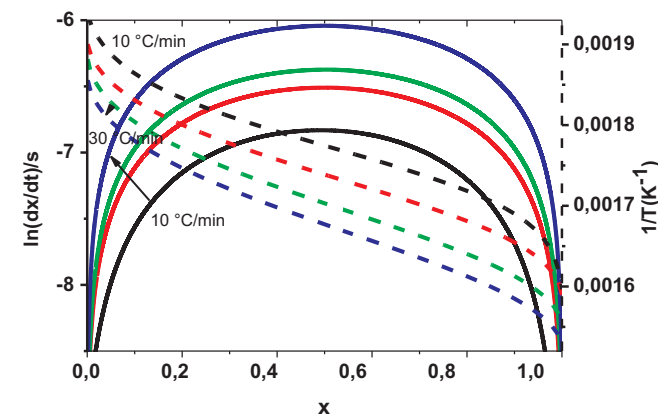

Fig. 5. $\ln(dx/dt)$ and $1/T$ versus of crystallized fraction x at different heating rates.

Table 4
Activation energy E_A and coefficient of determination R^2 for different crystallized fractions.

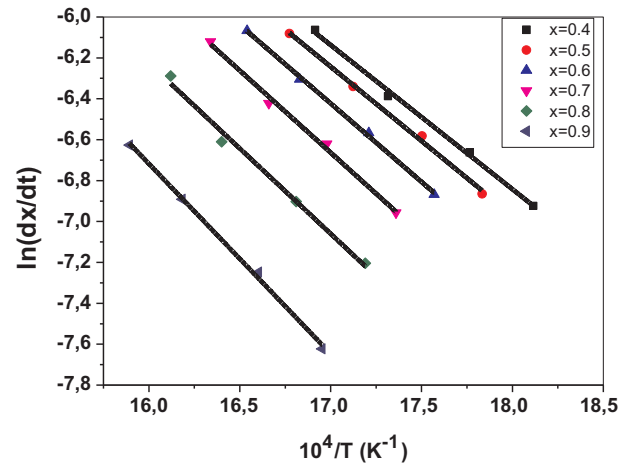| X	$E_A/(kJ \cdot mol^{-1})$	R^2
0.1	71.99	0.99
0.2	71.391	0.998
0.3	66.834	0.997
0.4	56.837	0.995
0.5	60.446	0.995
0.6	63.826	0.997
0.7	66.746	0.997
0.8	69.363	0.994
0.9	77.264	0.998

Fig. 6. $\ln(dx/dt)$ versus $1/T$ at same value of crystallized fraction x at different heating rates.

$$n = \frac{\ln[\ln(1-x_2)/\ln(1-x_1)]}{\ln[(1-x_2)\ln(1-x_2)/(1-x_1)\ln(1-x_1)]} \tag{19}$$

and the frequency factor k_0 can be calculated by the following equation:

$$\ln[k_0 f(x_1)] = \ln(k_0) + \ln(n) + \frac{n-1}{n}[\ln(-\ln(1-x))] + \ln(1-x) \tag{20}$$

The average of activation energy of formation of β ($Mg_{17}Al_{12}$) precipitate by isothermal techniques equal 67.18 kJ/mol agreement with that by non-isothermal techniques were around 62.02 kJ/mol. The values of Avrami parameters n are estimated by isothermal and non-isothermal approximately concurrence equal to 3.193 and 2.79, and the frequency factor k_0 is $1.24 \times 10^9 s^{-1}$. These values indicate that bulk nucleation with a constant number of nuclei was dominant in three-dimensional (polyhedron) controlled by interface reaction. These parameters are in a good concordance with works of Kabirian and Mahmudi [29,30].

The X-ray diffraction spectrum of the AZ91 alloy homogenized at 420 °C for 4 h, quenched rapidly with water and aged for 2 h at 170, 220, 270 and 320 °C, respectively, (Fig. 7). In the quenched state the X-ray diffraction spectrum shows only the peaks relative to the HC (P63/mmc) structure of the supersaturated solid solution α_0 (single-phase domain). The values of the crystalline parameters a = b (Mg) = 3.118 Å and c (Mg) = 5.118 Å, are very close to those mentioned in previous studies (a = b = 3.2088 Å, c = 5.2099 Å) [31]. After 2 h of aging at 170 °C, we show a small shift of these diffraction peaks towards the large nails and also gives low trace for the new phase precipitates β-$Mg_{17}Al_{12}$ (Fig. 8b). At 220, 270 and 320 °C temperatures of aging for 2 h, the XRD spectra show the existence of peaks of the β-$Mg_{17}Al_{12}$ precipitated phase with a high intensity and which increase with increasing aging temperatures, as the case may be peak of the family of planes (4 1 1)β (Fig. 8). In this case, the ratio of the lattice
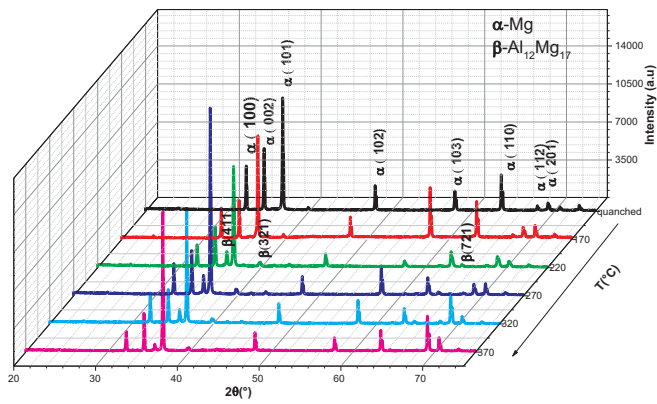
Fig. 7. X-ray spectra of the AZ91 alloy homogenized at 420 °C for 18 h quenched with water and aged for 2 h at 170, 220, 270, 320 and 370 °C.

Fig. 9. Effect of temperature on the c/a ratio of α (Mg) and lattice parameter of β-Mg$_{17}$Al$_{12}$ phase of AZ91 alloy.

parameter will be a/c = 3.62687 Å (Fig. 9). This value is expected because the output of the aluminum must decrease the value of the crystal lattice parameter. This is still justified for the case of aging for 2 h at 370 °C, it is noted that the intensity of the precipitate phase less than that of 220, 270 and 320 °C because we are close to magnesium phase
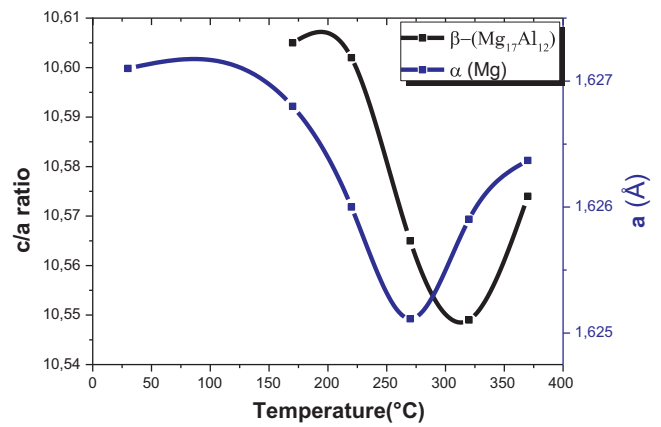
α$_0$(Mg) (the supersaturated phase) (Fig. 8f). It is noted that the kinetics of precipitation reaction is faster with the temperature range (220–370 °C) [32].

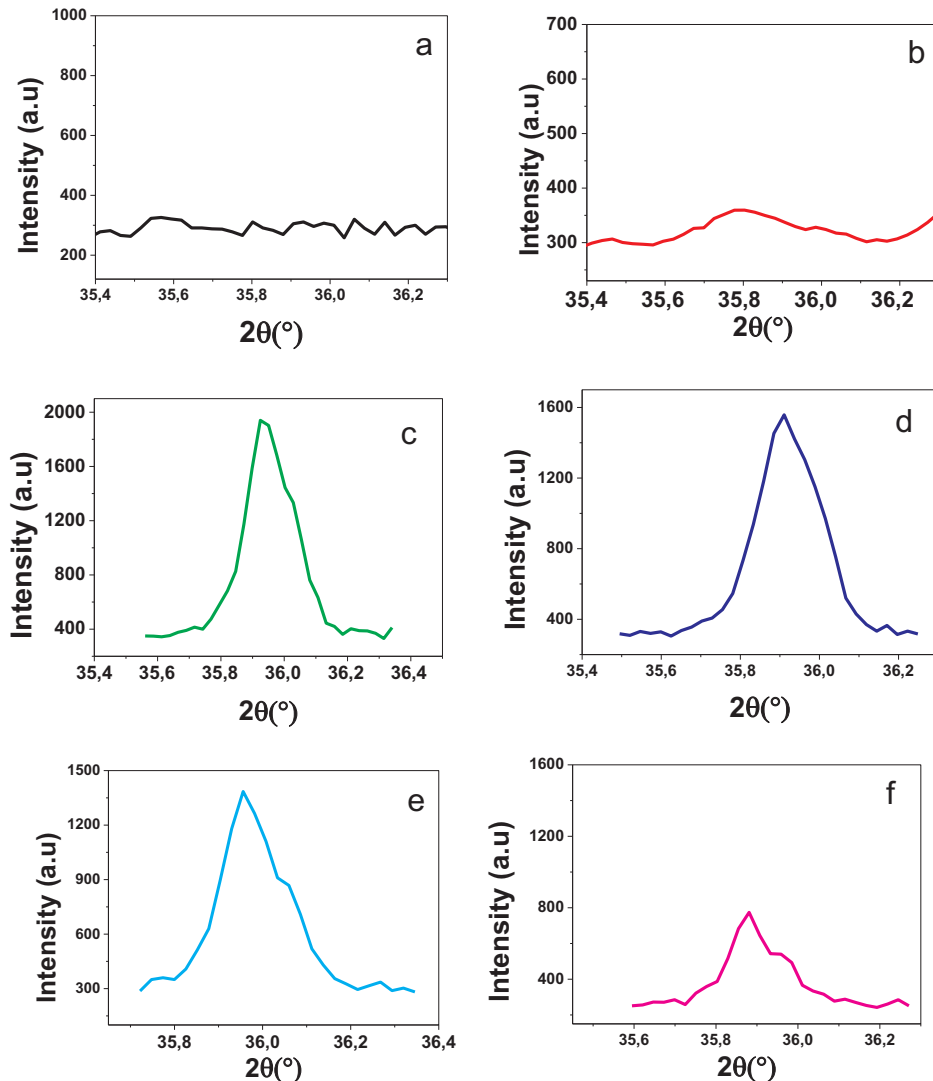The Vickers hardness testing of AZ91 quenched and aged at

Fig. 8. A part of the XRD spectra of the AZ91 alloy homogenized at 420 °C for 18 h quenched with water (a) and aged for 2 h at 170 (b), 220 (c), 270 (d), 320 (e) and 370 °C (f). (Presentation only the peak (4 1 1) of β-Mg$_{17}$Al$_{12}$ phase).
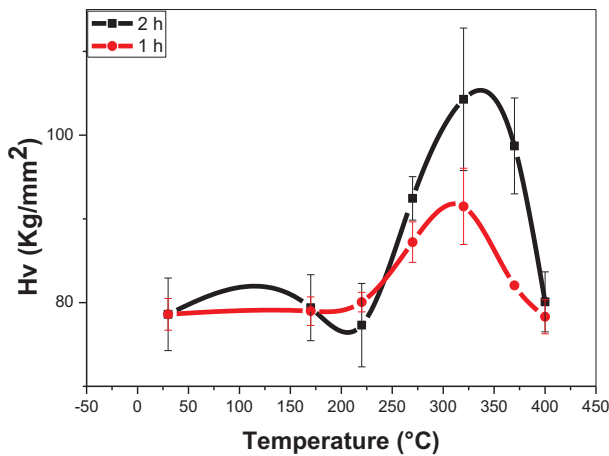
Fig. 10. Evolution of the micro-hardness Hv of AZ91 alloy, homogenized to 420 °C for 18 h, quenched in water and aged at the temperatures 170, 220, 270, 320 and 370 °C for 1 and 2 h.

different temperature, with non-isotherm (170–370 °C) for 1 and 2 h shown in (Fig. 10). The topical temperature to realize the maximum hardness approximately at 320 °C. The effect of temperature on the hardness are both increases from 220 to 270 °C, and decreases from 270 to 400 °C shown like peak, that is similar observation has been reported by the DSC experiment in current study (Fig. 1), this is caused by the formation of stable phase β-$Mg_{17}Al_{12}$ precipitate.

Conclusions

This study investigated the effect of aging temperature and time on the kinetics of precipitation of β-($Mg_{17}Al_{12}$) phase in AZ91 Alloy. It is found that the kinetics of the decomposition reaction is lower in the temperature range between 220 and 370 °C. The activation energies, measured after isothermal and non-isothermal treatments by five methods were around 67.18 and 62.02 kJ/mol, respectively. The Avrami parameter n of growth morphology reaction, by using the no-isothermal and isothermal treatments was around 3.19 and 2.79 respectively. We notice that the exponent n is between 2 and 3 so it is kinetics that under mixed control: reaction at the interface and diffusion. We mentioned in Section 2; that there is an aging which presents two modes of precipitation; cellular and continuous hence this kinetics with two phenomena taking place at almost the same time. Finally, the frequency factor calculated using the isothermal treatment is 1.24 $10^9 s^{-1}$.

Appendix A. Supplementary material

Supplementary data associated with this article can be found, in the online version, at https://doi.org/10.1016/j.rinp.2018.07.009.

References

[1] Mordike B, Ebert T. Magnesium: properties—applications—potential. Mater Sci Eng, A 2001;302(1):37–45.
[2] Adamson K, Tawil D. Magnesium and magnesium alloys, in Corrosion. 3rd ed. 1994, Elsevier: p. 4: 98–4: 115.
[3] Cerri E, Barbagallo S. The influence of high temperature exposure on aging kinetics of a die cast magnesium alloy. Mater Lett 2002;56(5):716–20.
[4] Srinivasan A. Observations of microstructural refinement in Mg–Al–Si alloys containing strontium. J Mater Sci 2006;41(18):6087–9.
[5] Celotto S. TEM study of continuous precipitation in Mg–9 wt% Al–1 wt% Zn alloy. Acta Mater 2000;48(8):1775–87.
[6] Bamberger M, Dehm G. Trends in the development of new Mg alloys. Annu. Rev. Mater. Res. 2008;38:505–33.
[7] Clark J. Age, hardening in a Mg-9 wt.% Al alloy. Acta Metall 1968;16(2):141–52.
[8] Nayeb-Hashemi A, Clark J. The Mg − Mn (Magnesium-Manganese) system. Bulletin Alloy Phase Diagr 1985;6(2):160–4.
[9] Sakkinen DJ. Physical metallurgy of magnesium die cast alloys. SAE Trans, 994; p. 558–69.
[10] Bastow TJ, Smith ME. Observation of precipitation in Mg-Al alloys by 25Mg and 27Al NMR. J Phys: Condens Matter 1995;7(25):4929.
[11] Tkacz J, Minda J, Fintová S, Wasserbauer J. Comparison of electrochemical methods for the evaluation of cast AZ91 magnesium alloy. Materials 2016;9:925.
[12] Azzeddine H, Abdessameud S, Sari A, Alili B, Bradai D. Kinetics of the precipitation AZ91, Kinetics of the precipitation in AZ91 alloy through in situ X-ray diffraction. Cinétique de la précipitation dans l'alliage AZ91 par la diffraction des rayons X in situ Phys. Chem. News 2009;49:109–13.
[13] Tu KN, Turnbull D. Morphology of cellular precipitation of tin from lead-tin bi-crystals. Acta Mater 1967;15:369–76.
[14] Clark JB, Age,. hardening in a Mg-9 wt.% Al alloy. Acta Metall 1968;16:141–52.
[15] Braszczyńska-Malik KN. Discontinuous and continuous precipitation in magnesium–aluminium type alloys. J Alloy Compd 2009;477:870–6.
[16] Ke W, Han EH, Han YF, Kainer K, Luo AA. Magnesium – science, technology and applications. Mat Sci Forum 2004:488–9. p. 9–16.
[17] Zeng R. Precipitation hardening in AZ91 magnesium alloy. University of Birmingham; 2013. PhD Thesis.
[18] Augis J, Bennett J. Calculation of the Avrami parameters for heterogeneous solid state reactions using a modification of the Kissinger method. J Therm Anal Calorim 1978;13(2):283–92.
[19] Johnson WA. Reaction kinetics in process of nucleation and growth. Trans AIME 1939;135:416–58.
[20] Bansal NP. Kinetics of crystallization of ZrF4-Ba2-LaF3 glass by differential scanning calorimetry. J Am Ceram Soc 1983;66(4):233–8.
[21] Blaine RL, Kissinger HE. Homer Kissinger and the Kissinger equation. Thermochim Acta 2012;540:1–6.
[22] Kissinger HE. Variation of peak temperature with heating rate in differential thermal analysis. J Res National Bureau Stand 1956;57(4):217–21.
[23] Boswell P. On the calculation of activation energies using a modified Kissinger method. J Therm Anal Calorim 1980;18(2):353–8.
[24] Mahadevan S, Giridhar A, Singh A. Calorimetric measurements on as-sb-se glasses. J Non-Cryst Solids 1986;88(1):11–34.
[25] Ozawa T. A new method of analyzing thermogravimetric data. Bulletin Chem Soc Japan 1965;38(11):1881–6.
[26] Donoso E, Varschavsky A. Microcalorimetric Evaluation of Precipitation in Cu–2Be–0.2Mg. J Therm Anal Calorim 2001;63:249–66.
[27] Matusita K, Sakka S. Kinetic study of crystallization of glass by differential thermal analysis—criterion on application of Kissinger plot. J Non-Cryst Solids 1980;38:741–6.
[28] Fatmi M, Ghebouli B, Ghebouli MA, Chihi T, Hafiz A. The kinetics of precipitation in Al-2.4 wt% Cu alloy by Kissinger, Ozawa, Bosswel and Matusita methods. Physica B 2011;406:2277–80.
[29] Kabirian F, Mahmudi R. Effects of rare earth element additions on the impression creep behavior of Az91 magnesium alloy. Metall Mater Trans A 2009;40(9):2190–201.
[30] Kabirian F, Mahmudi R. Effects of Zr additions on the microstructure and impression creep behavior of Az91 magnesium alloy. Metall Mater Trans A 2010;41(13):3488–98.
[31] Busk RS. Effect of temperature on the lattice parameters of magnesium alloys. JOM 1952;4(2):207–9.
[32] Papamantellis S, Penelope, Fischer P. Neutron diffraction investigation of atomic distribution on $Mg_{17}Al_{12}$. Naturwissenschaften 1970;57(3):128–9.